

**Strain-driven disproportionation at a correlated oxide metal-insulator transition**T. H. Kim<sup>1</sup>, T. R. Paudel<sup>2</sup>, R. J. Green<sup>3,4</sup>, K. Song<sup>5</sup>, H.-S. Lee<sup>5</sup>, S.-Y. Choi<sup>6</sup>, J. Irwin<sup>7</sup>, B. Noesges<sup>8</sup>, L. J. Brillson<sup>8</sup>,  
M. S. Rzchowski<sup>7</sup>, G. A. Sawatzky<sup>3</sup>, E. Y. Tsybal<sup>2</sup>, and C. B. Eom<sup>1,\*</sup><sup>1</sup>*Department of Materials Science and Engineering, University of Wisconsin–Madison, Madison, Wisconsin 53706, USA*<sup>2</sup>*Department of Physics and Astronomy and Nebraska Center for Materials and Nanoscience,  
University of Nebraska, Lincoln, Nebraska 68588, USA*<sup>3</sup>*Quantum Matter Institute, Department of Physics and Astronomy, University of British Columbia,  
Vancouver, British Columbia, Canada V6T 1Z4*<sup>4</sup>*Department of Physics and Engineering Physics, University of Saskatchewan, Saskatoon, Saskatchewan, Canada S7N 5E2*<sup>5</sup>*Materials Modeling and Characterization Department, Korea Institute of Materials Science, Changwon 51508, Republic of Korea*<sup>6</sup>*Department of Materials Science and Engineering, Pohang University of Science and Technology, Pohang 37673, Republic of Korea*<sup>7</sup>*Department of Physics, University of Wisconsin–Madison, Madison, Wisconsin 53706, USA*<sup>8</sup>*Departments of Physics and Electrical & Computer Engineering, The Ohio State University, Columbus, Ohio 43210, USA*

(Received 20 June 2017; accepted 22 January 2020; published 9 March 2020)

Metal-to-insulator phase transitions in complex oxide thin films are exciting phenomena which may be useful for device applications, but in many cases the physical mechanism responsible for the transition is not fully understood. Here we demonstrate that epitaxial strain generates local disproportionation of the  $\text{NiO}_6$  octahedra, driven through changes in the oxygen stoichiometry, and that this directly modifies the metal-to-insulator phase transition in epitaxial (001)  $\text{NdNiO}_3$  thin films. Theoretically, we predict that the Ni-O-Ni bond angle decreases, while octahedral tilt and local disproportionation of the  $\text{NiO}_6$  octahedra increases resulting in a small band gap in an otherwise metallic system. This is driven by an increase in oxygen vacancy concentration in the rare-earth nickelates with increasing in-plane biaxial tensile strain. Experimentally, we find an increase in pseudocubic unit-cell volume and resistivity with increasing biaxial tensile strain, corroborating our theoretical predictions. With electron-energy-loss spectroscopy and x-ray absorption, we find a reduction of the Ni valence with increasing tensile strain. These results indicate that epitaxial strain modifies the oxygen stoichiometry of rare-earth perovskite thin films and through this mechanism affects the metal-to-insulator phase transition in these compounds.

DOI: [10.1103/PhysRevB.101.121105](https://doi.org/10.1103/PhysRevB.101.121105)

Metal-to-insulator phase transitions (MITs) in strongly correlated electronic systems are fascinating phenomena which have attracted significant attention for decades [1]. Among complex oxide materials which exhibit MITs are rare-earth nickelates having the generic formula  $\text{RNiO}_3$ , where the rare-earth element ( $R$ ) is smaller than lanthanum, i.e.,  $R = \text{Pr}, \text{Nd}, \dots$  [2]. The critical temperature of the MIT is dependent on the Ni-O-Ni bond angle: straightening the angle with a larger  $R$  cation stabilizes the metallic state over the insulating state and lowers the transition temperature [3–5]. For example, the MIT temperatures in bulk  $\text{NdNiO}_3$  and  $\text{SmNiO}_3$  (Ni-O-Ni bond angles of  $157.1^\circ$  and  $153.4^\circ$ , respectively) have been reported to be approximately 200 and 400 K, respectively. It should be also emphasized that a breathing order by disproportionation of the Ni-O bond length plays a crucial role in the MIT [6–10].

In  $\text{RNiO}_3$  thin films, misfit strain arising from a lattice mismatch between the film layer and the underlying substrate affects the lattice volume, electrical conductivity, and MIT temperature [11–18]. In particular, films under in-plane tensile strain are more insulating compared to those under in-plane

compressive strain. The origin of this interesting phenomenon remains unclear, although a number of mechanisms have been proposed [19–24]. We also note that the effect of oxygen nonstoichiometry on the MIT has been reported in bulk  $\text{RNiO}_3$  [25,26].

It is widely accepted that epitaxial strain in transition-metal oxide films can be accommodated through the formation of oxygen vacancy defects, resulting in off-stoichiometry of the compound [27]. Thus, cation/oxygen stoichiometry is an important factor involved with physical and functional properties of complex oxide films [2,28]. A missing cation or oxygen at a given lattice site modifies the local charge/spin/orbital configuration, critically affecting material properties. There have been recent studies on how such vacancy defects inducing off-stoichiometry influence the structural, electronic, magnetic, and transport characteristics of complex oxide films [27–34]. It is therefore possible that the experimentally observed strain-driven changes in the lattice volume, electrical conductivity, and MIT temperature of  $\text{RNiO}_3$  thin films [11–18] are mediated by off-stoichiometry resulting from the formation of oxygen vacancies. Answering this question is of great significance for the understanding of a broader range of phenomena occurring in complex oxide thin films subject to epitaxial strain.

\*ceom@wisc.edu

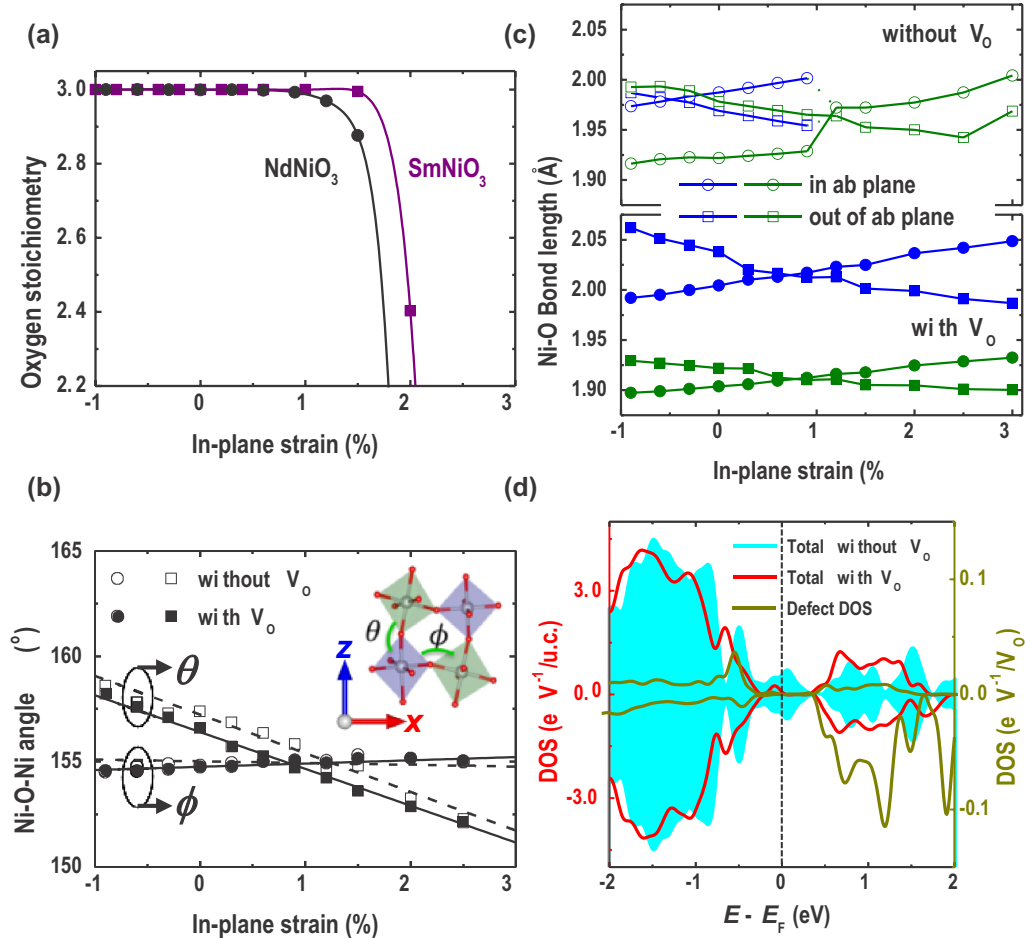


FIG. 1. (a) Strain-dependent oxygen stoichiometry in NdNiO<sub>3</sub> (solid circles) and SmNiO<sub>3</sub> (solid squares). The stoichiometry is calculated at room temperature and thermal equilibrium with O<sub>2</sub> molecule. The lines are guides to the eye for the data points. (b) Calculated octahedral tilt ( $\theta$ ) and rotation ( $\phi$ ) angles as a function of in-plane strain. The inset shows a *Pbnm*NdNiO<sub>3</sub> unit cell indicating the angles  $\theta$  and  $\phi$ . The tilt angle  $\theta$  and rotation angle  $\phi$  represent the Ni-O-Ni bonding angles with respect to the  $z$  axis and in the  $xy$  in-plane, respectively. In (b), open (filled) symbols represent the quantities in the absence (presence) of oxygen vacancies. (c) Calculated shorter (green) and longer (blue) Ni-O bond lengths in the  $a-b$  plane (circle) and the  $c$  plane (square) in the absence (open symbol) and presence (filled symbol) of oxygen vacancy. Note that the difference between the shorter and longer Ni-O bondings increases in the presence of oxygen vacancy. (d) Total and local density of states (DOS) in NdNiO<sub>3</sub> projected at the defect sites in the presence (lines) and absence (cyan background) of oxygen vacancies. Note a band gap for the oxygen-deficient NdNiO<sub>3</sub>.

In this work, we present the strain-dependent formation of oxygen vacancies and their impact on the metal-to-insulator phase transition in  $R\text{NiO}_3$  ( $R = \text{Nd, Sm}$ ) (001) thin films. Theory predicts that oxygen vacancies can be created to accommodate biaxial tensile strain in  $R\text{NiO}_3$  films. The oxygen vacancies drive long-ranged structural and electronic modifications, which enhance disproportionation of the NiO<sub>6</sub> octahedra stabilizing the insulating phase [35]. Experiment observes that the pseudocubic unit-cell volume and resistivity in epitaxial  $R\text{NiO}_3$  films increase with biaxial tensile strain, which is consistent with our theoretical predictions. It is highly likely that the strain-induced oxygen vacancies produce a more ionic Ni<sup>2+</sup> state and enhance the local disproportionation. Our results reveal that oxygen stoichiometry susceptible to epitaxial strain can be a key factor to figure out the metal-to-insulator transition in complex oxide thin films.

In order to address the above issue, we performed density-functional theory (DFT) calculations. Our theoretical results show that oxygen stoichiometry in  $R\text{NiO}_3$  is very sensitive

to in-plane biaxial strain [Fig. 1(a)]. The maximum oxygen vacancy formation energy (calculated using chemical potential corresponding to O<sub>2</sub> molecule/ $R\text{NiO}_3$  in the dilute limit) decreases as the in-plane strain increases (Supplemental Material Fig. S1) [36] (see also Refs. [37–44] therein). For in-plane tensile strain above 1.9% (2.2%), the formation energy of an oxygen vacancy in NdNiO<sub>3</sub> (SmNiO<sub>3</sub>) becomes negative and therefore, the materials become largely oxygen deficient at large tensile strain [Fig. 1(a)], while they are stoichiometric for compressive strain.

Further, we find that an oxygen vacancy is more easily formed in the NiO<sub>2</sub> plane than in the RO ( $R = \text{Nd, Sm}$ ) plane of the  $R\text{NiO}_3$  unit cell (Supplemental Material Fig. S2) [36]. When the oxygen atom connecting two octahedra is removed in the NiO<sub>2</sub> plane, both in-plane octahedra tilt toward each other [Fig. 1(b)]. The oxygen octahedral structure of bulk NdNiO<sub>3</sub> is represented by the tilt angle  $\theta$  with respect to the  $z$  axis and rotation angle  $\phi$  in the  $xy$  in-plane [the inset of Fig. 1(b)]. As in-plane biaxial strain increases,  $\theta$  clearly

decreases, while  $\phi$  remains nearly constant, indicating the predominant effect of strain on octahedral tilting [45]. In the presence of oxygen vacancies,  $\text{NiO}_6$  octahedra in  $\text{RNiO}_3$  are more tilted, as reflected in smaller  $\theta$  values, whereas  $\phi$  is approximately unchanged.

In addition to octahedral rotations and tilts, we also observe disproportionation of the  $\text{NiO}_6$  octahedra. There are two inequivalent octahedra [inset in Fig. 1(b)] with shorter and longer Ni-O bond lengths, as shown in Fig. 1(c). For stoichiometric  $\text{NdNiO}_3$  [Fig. 1(c), top panel], our DFT calculations indicate that this disproportionation decreases with the increasing in-plane biaxial strain and eventually vanishes making the two octahedra equivalent beyond an epitaxial strain of 1%, at which two different Ni-O bonds in the  $a-b$  plane and the  $c$  plane at compressive strain merge to a single  $a-b$  plane and  $c$ -plane Ni-O bonds. In the presence of oxygen vacancies [Fig. 1(c), lower panel], the disproportionation is more pronounced, and persists for all investigated levels of strain.

This change in disproportionation with oxygen vacancy dramatically affects the overall electronic properties. The cyan background in Fig. 1(d) shows the zero strain, stoichiometric, total density of states (DOS). It indicates an overall metallicity, with near band-edge states that are dominated by mixed O-2*p* and Ni-3*d* bands. The solid red line in the same panel shows the opening of a band gap when oxygen vacancies are included, driving a metal-insulator transition. The DOS (the dark-yellow line) shows that occupied defect states lie in the valence band of the host material and, hence, the defect-induced effects are long ranged. This is in contrast to wide band gap semiconductors where defect states lie in the band gap and their effect is short ranged. The long-ranged effect of oxygen vacancies promotes the octahedral tilting and produces additional disproportionation and drives the system into the insulating state. The metallicity of the defect-free system suggests that the DFT does not completely capture the electronic properties, but the calculation clearly indicates that vacancy-induced disproportionation drives the system toward the insulating state, which would result in a higher MIT temperature. For  $\text{SmNiO}_3$ , the DFT calculations show qualitatively analogous behavior.

To study the effect of in-plane biaxial strain on oxygen stoichiometry, lattice structures, and electronic properties, we grew epitaxial  $\text{RNiO}_3$  ( $R = \text{Nd, Sm}$ ) (001) films using pulsed laser deposition (PLD) with *in situ* monitoring by reflection high-energy electron-diffraction (RHEED). During the PLD growth of  $\text{RNiO}_3$  (001) films, RHEED oscillations were used to estimate the film thickness (Supplemental Material Fig. S3) [36]. In Fig. 2(a), atomic force microscopy (AFM) topography and RHEED pattern images show that the as-grown  $\text{NdNiO}_3$  (14 nm) films have atomically flat surfaces with a clear step-terrace structure and high-crystalline qualities, respectively. As depicted in Fig. 2(b),  $\text{LaAlO}_3$  (LAO) (001),  $\text{NdGaO}_3$  (NGO) (110), and  $\text{SrTiO}_3$  (STO) (001) substrates were used to investigate epitaxial films in a wide range of strain states. Note that the pseudocubic lattice constants of bulk  $\text{NdNiO}_3$  and  $\text{SmNiO}_3$  are 3.808 and 3.801 Å, respectively [5]. Thus, the lattice mismatch of an  $\text{NdNiO}_3$  ( $\text{SmNiO}_3$ ) film is  $-0.5\%$  ( $-0.3\%$ ), 1.3% (1.5%), and 2.5% (2.7%) with respect to pseudocubic LAO, NGO, and STO substrates, respectively;

that is, under in-plane compressive strain for the LAO substrate and under in-plane tensile strain for the NGO and STO substrates. To identify the coherency and actual strain states, reciprocal space mappings (RSMs) around the pseudocubic  $(-103)$  Bragg peaks were performed, as shown in Fig. 2(c) [for  $\text{SmNiO}_3$  (001) films, see Supplemental Material Fig. S4(a)] [36]. These show that the films are coherent with respect to the underlying substrate and strained with the same in-plane lattice constant as that of the substrate in pseudocubic notation. By deriving a pseudocubic unit-cell volume from the measured lattice constants, we also examined the relation between structural properties and oxygen off-stoichiometry in  $\text{RNiO}_3$  films.

As evident from Fig. 2(d), the pseudocubic unit-cell volume of  $\text{RNiO}_3$  films increases with in-plane tensile strain, whereas it is identical to the bulk value for in-plane compressive strain (Supplemental Material Table S1) [36]. We found that the measured out-of-plane lattice constants deviate from those calculated assuming the volume conservation of  $\text{RNiO}_3$  unit cells. This difference between the measured and calculated lattice constants gets larger with in-plane tensile strain, indicative of a volume expansion (Supplemental Material Fig. S5) [36]. The volume expansion of  $\text{RNiO}_3$  unit cells by in-plane tensile strain is also confirmed in atomic-scale scanning transmission electron microscopy (STEM) measurements (Supplemental Material Fig. S6) [36]. It is further interesting that an  $\text{NdNiO}_3$  film on a STO substrate (a lattice mismatch of +2.5%) is coherent with a volume expansion, whereas an  $\text{NdNiO}_3$  film on a  $\text{YAlO}_3$  substrate (a lattice mismatch of  $-2.7\%$ ) is relaxed, preserving the unit-cell volume (Supplemental Material Fig. S7) [36]. For  $\text{NdNiO}_3$  and  $\text{SmNiO}_3$  films grown on STO (001) substrates, their unit-cell volumes increase up to 4.4% and 6.1%, respectively. *Albeit* the strain dependence of the Poisson's ratio is considered, this volume change in  $\text{RNiO}_3$  films is too large. Note that the Poisson's ratio in complex oxides is usually in the range of 0.2–0.3 [46,47]. This is suggestive of a change in oxidation state under tensile strain, but not compressive strain. Similar volume expansion by in-plane tensile strain has been previously reported in other transition-metal oxide films where multiple oxidation states of the transition-metal element are allowed [48,49].

We also found that electronic transport properties strongly depend on epitaxial strain. Figure 2(e) shows the temperature dependence of resistivity in the 14-nm-thick  $\text{NdNiO}_3$  (001) films.  $\text{NdNiO}_3$  samples undergo an explicit MIT as the temperature decreases. It is evident that  $\text{NdNiO}_3$  films under in-plane tensile strain (grown on NGO and STO substrates) exhibit larger resistivity than those under in-plane compressive strain (grown on a LAO substrate) at all temperatures. In  $\text{SmNiO}_3$  films, similar transport behaviors are observed [Supplemental Material Fig. S4(b)] [36]. In particular, the MIT in the tensile-strained  $\text{NdNiO}_3$  films occurs at a higher temperature, whereas it is suppressed in the compressive-strained  $\text{NdNiO}_3$  films with a lower MIT temperature (Supplemental Material Fig. S8) [36]. And, the  $\text{NdNiO}_3$ /LAO film with better electrical conductivity gave higher carrier concentrations of mobile charges than the  $\text{NdNiO}_3$ /STO film (Supplemental Material Fig. S9) [36]. These strain-dependent transport properties are consistent with previous reports [11–14,17,18].

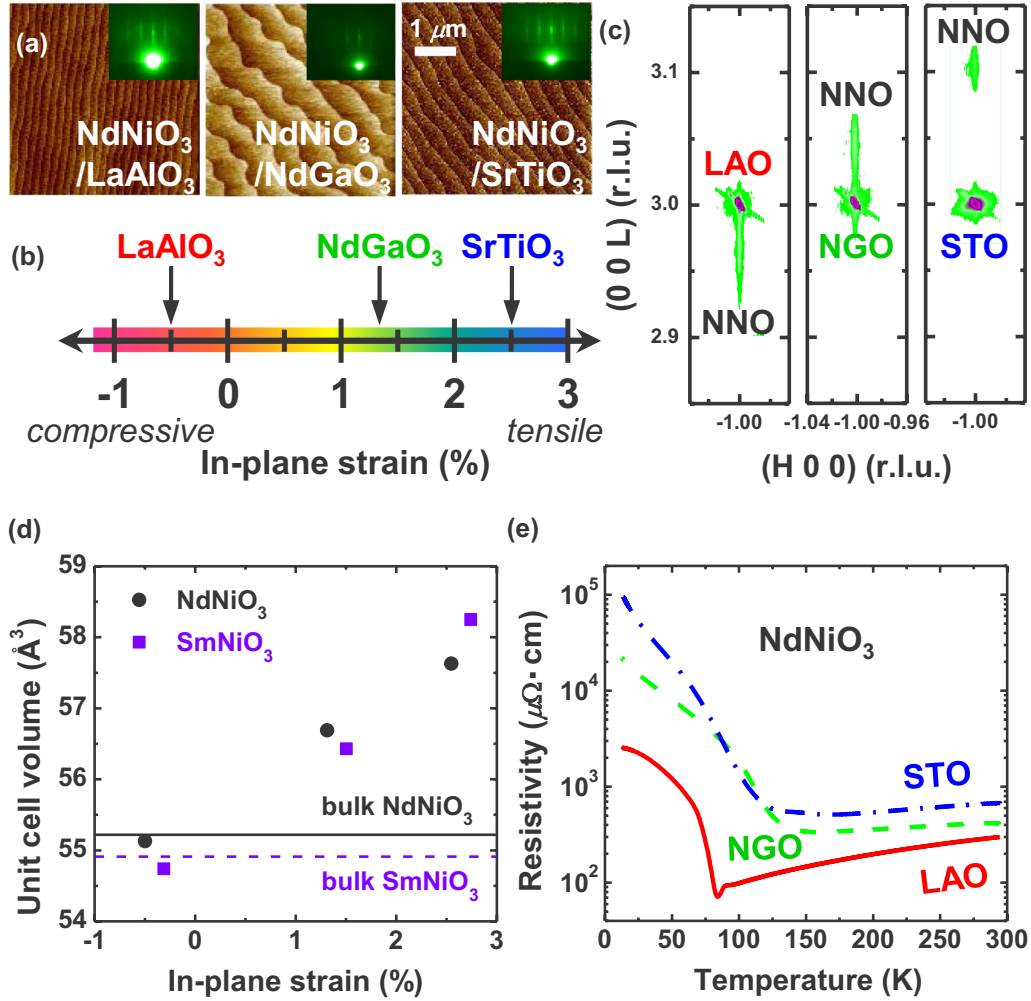


FIG. 2. (a) AFM topography images of the as-grown 14-nm-thick (left) NdNiO<sub>3</sub>/LaAlO<sub>3</sub> (LAO), (middle) NdNiO<sub>3</sub>/NdGaO<sub>3</sub> (NGO), and (right) NdNiO<sub>3</sub>/SrTiO<sub>3</sub> (STO) thin films, where the insets represent the corresponding RHEED patterns. (b) In-plane biaxial strain of NdNiO<sub>3</sub> with respect to pseudocubic LAO, NGO, and STO (001) substrates. (c)  $(-103)$  RSMs of pseudocubic NdNiO<sub>3</sub> (001) films. All of the RSMs are on the same scale in the  $H$  and  $L$  directions. All NdNiO<sub>3</sub> films are coherent with respect to the substrates. (d) The strain-dependent pseudocubic unit-cell volumes of epitaxial NdNiO<sub>3</sub> (solid circles) and SmNiO<sub>3</sub> (solid squares) films. The solid and dashed lines represent the unit-cell volume of bulk NdNiO<sub>3</sub> and SmNiO<sub>3</sub> in pseudocubic notation, respectively. (e) The temperature-dependent resistivity in the 14-nm-thick NdNiO<sub>3</sub> (001) films.

Strain-induced oxygen vacancies increase a pseudocubic unit-cell volume and resistivity in  $R\text{NiO}_3$  films. By carrying out cathodoluminescence (CL) measurements of our as-grown NdNiO<sub>3</sub> (001) films (Supplemental Material Fig. S10) [36], we first found that the formation of oxygen vacancies in  $R\text{NiO}_3$  films is quite dependent on the in-plane biaxial strain. In the tensile-strained NdNiO<sub>3</sub> films (i.e., NdNiO<sub>3</sub>/NdGaO<sub>3</sub> and NdNiO<sub>3</sub>/SrTiO<sub>3</sub> films) unlike the compressive-strained NdNiO<sub>3</sub>/LaAlO<sub>3</sub> film, we only observed distinct CL signals at the low photon energies of 1.8 eV which are directly related with oxygen-vacancy-mediated optical transitions [50,51]. By visualizing oxygen atoms in annular bright field-STEM images of NdNiO<sub>3</sub>/STO and NdNiO<sub>3</sub>/LAO films, we also verified that the tensile-strained NdNiO<sub>3</sub> film is more oxygen deficient than the compressive-strained NdNiO<sub>3</sub> film (Supplemental Material Fig. S11) [36]. Then, by performing *in situ* annealing experiments of as-deposited NdNiO<sub>3</sub> films in different oxygen-ambient

environments, it was further identified that more oxygen-deficient NdNiO<sub>3</sub> films exhibit a larger unit-cell volume in pseudocubic notation and higher resistivity (Supplemental Material Fig. S12) [36]. A possibility of cation vacancies in this volume expansion could be excluded by examining the cation stoichiometry of as-grown NdNiO<sub>3</sub> films using Rutherford backscattering spectrometry (Supplemental Material Fig. S13) [36]. For two NdNiO<sub>3</sub> films, one with in-plane compressive strain and the other with in-plane tensile strain, the ratio of chemical composition between Nd and Ni atoms is 1:1 within measurement errors. It is highly likely that the oxygen vacancy concentration in tensile-strained  $R\text{NiO}_3$  films is higher than that in compressive-strained  $R\text{NiO}_3$  films. Then, the greater amount of oxygen vacancy defects in the tensile-strained  $R\text{NiO}_3$  films leads to further enlarged volume and further enhanced resistivity.

We observe a reduction of Ni valence state in 10-unit-cell-thick NdNiO<sub>3</sub> (3.8 nm) films under in-plane tensile strain



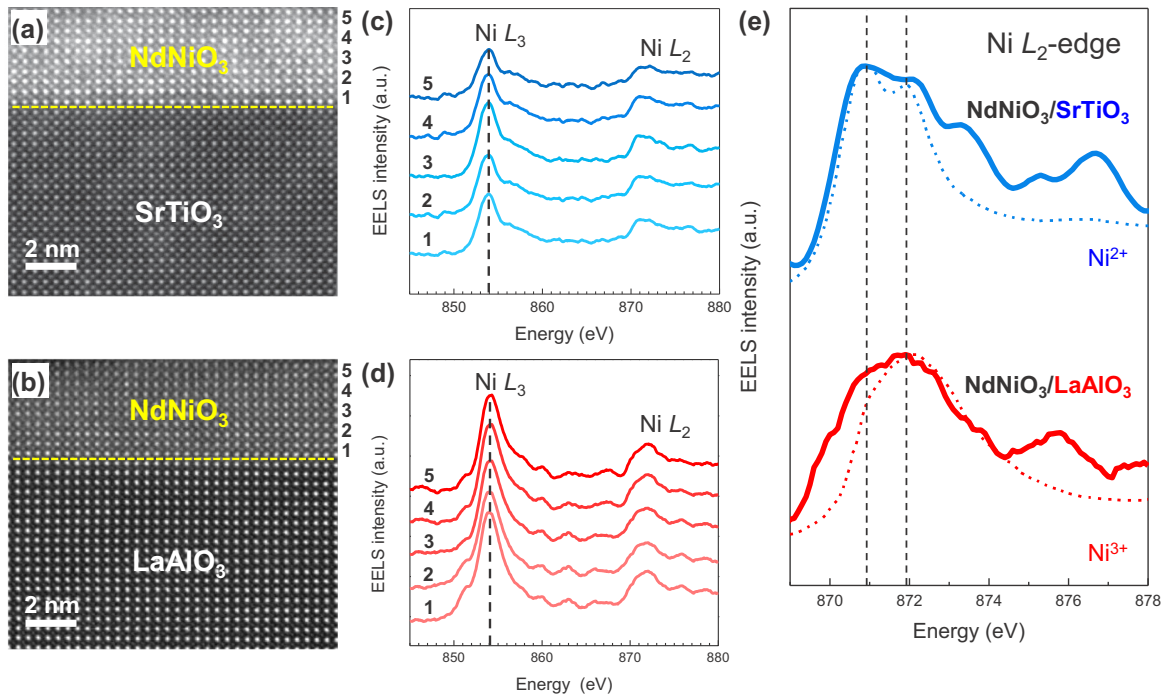


FIG. 3. STEM–high-angle annular dark-field images of the 10-unit-cell-thick NdNiO<sub>3</sub> (3.8 nm) films grown on (a) STO and (b) LAO substrates along the pseudocubic [100] zone axis. (c),(d) EELS spectra of Ni  $L_{2,3}$  edges obtained across the NdNiO<sub>3</sub> films shown in (a) and (b), respectively. Black dashed and gray dotted lines are guidelines for Ni  $L_3$ . (e) The Ni  $L_2$  edges of the NdNiO<sub>3</sub>/STO (the blue solid line) and NdNiO<sub>3</sub>/LAO (the red solid line) films in (c) and (d), respectively. A comparison with the EELS calculation spectra of Ni<sup>2+</sup> (blue dashed line) and Ni<sup>3+</sup> (red dashed line) evidences that the oxidation states of Ni in 10-unit-cell-thick NdNiO<sub>3</sub> films grown on STO and LAO substrates are more toward Ni<sup>2+</sup> and Ni<sup>3+</sup>, respectively. For Ni<sup>2+</sup>, two distinct peaks (870.8 and 871.9 eV) were calculated with the estimated crystal-field splitting parameter,  $10Dq$ , 1.1 eV, while three peaks (870.1, 871.9, and 873.8 eV) with higher  $10Dq$ , 1.8 eV were found in the Ni<sup>3+</sup> state.

using the atomic-resolved STEM and electron-energy-loss spectroscopy (EELS) techniques. For two epitaxial NdNiO<sub>3</sub> thin films with atomically sharp interfaces grown on STO (2.5% in-plane tensile strain) and LAO (0.5% in-plane compressive strain) (001) substrates, as shown in Figs. 3(a) and 3(b), the Ni  $L_{2,3}$  edges were measured over the film thickness [Figs. 3(c) and 3(d)]. All EELS spectra in each NdNiO<sub>3</sub> (001) film are similar with respect to the thickness, which indicates that the electronic and chemical states of Ni in the as-grown NdNiO<sub>3</sub> film are spatially homogeneous throughout the whole thickness. On the other hand, the comparison of Ni  $L_2$  edges between NdNiO<sub>3</sub>/STO and NdNiO<sub>3</sub>/LAO films [Fig. 3(e)] makes sure that the valence states of Ni cations are strongly correlated with the in-plane biaxial strain. Further confirmation with EELS calculation of Ni<sup>2+</sup> and Ni<sup>3+</sup> valence states reveals that the oxidation states of Ni cations in the NdNiO<sub>3</sub>/STO and NdNiO<sub>3</sub>/LAO films are more toward ionic Ni<sup>2+</sup> and covalent Ni<sup>3+</sup>, respectively [36] (see also Refs. [52,53] therein).

Figure 4 shows Ni  $L_{2,3}$  x-ray absorption spectroscopy (XAS) data for the 10-unit-cell-thick NdNiO<sub>3</sub> (3.8 nm) films on different substrates. For each case, spectra are measured at 22 K, where the nickelate films are insulating. In the insulating phase, a two-peaked structure is present at the Ni  $L_3$  edge (between  $\sim 853$  and  $\sim 854$  eV). It is interesting that the XAS spectra of the NdNiO<sub>3</sub> films become closer to that of NiO, as

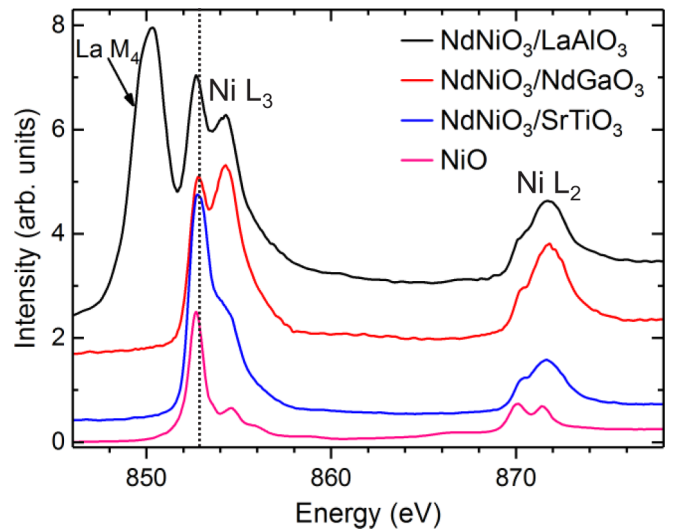


FIG. 4. Ni  $L_{2,3}$  x-ray absorption spectroscopy (XAS) of the 10-unit-cell-thick NdNiO<sub>3</sub> (3.8 nm) films on LAO, NGO, and STO substrates at 22 K. All spectra are measured via the total fluorescence yield mode, which is bulk sensitive with a probing depth of several tens of nanometers. The XAS spectra of the NdNiO<sub>3</sub> films become closer to that of NiO, as the substrate changes from LAO to NGO to STO, indicative of the reduction of Ni charge valence toward ionic Ni<sup>2+</sup> by in-plane tensile strain.

the substrate changes from LAO to NGO to STO. While the first sharp peak (denoted by the dotted line in Fig. 4) is an intrinsic feature of the nickelate spectrum [6,54–56], the identical and sharp  $L_3$  peak of  $\text{Ni}^{2+}$  in NiO shifts negligibly lower in energy. In thicker (14 nm) nickelate films [Supplemental Material Fig. S14(a)] [36], though there is slightly less  $\text{Ni}^{2+}$  observed via XAS, a similar increase in the first peak intensity is observed for increasing tensile strain. This indicates that the Ni valence is reduced toward  $\text{Ni}^{2+}$  for tensile strain. In an oxygen-deficient  $\text{NdNiO}_3$  film, the reduction of the Ni valence state is more pronounced (Supplemental Material Fig. S15) [36]. Oxygen vacancies formed to accommodate in-plane tensile strain reduce the oxidation state of Ni cations from the covalent  $\text{Ni}^{3+}$  to the ionic  $\text{Ni}^{2+}$  in  $\text{NdNiO}_3$  (001) films, which promotes disproportionation of Ni  $3d$ –O  $2p$  hybridization [Supplemental Material Figs. S14(b) and S14(c)] [36].

In conclusion, we have demonstrated that strain-driven changes in structural distortion, lattice volume, electrical conductivity, and MIT temperature of epitaxially grown rare-earth nickelate films are mediated by chemical off-stoichiometry resulting from the formation of oxygen vacancies. This result is of significance for a fundamental understanding of a broader range of physical properties and phenomena oc-

curing in complex oxide thin films subject to epitaxial strain.

This work was supported by the National Science Foundation (NSF) under DMREF Grants No. DMR-1629270 and No. DMR-18-00130. The research at University of Nebraska–Lincoln was supported by the NSF through the Nebraska Materials Research Science and Engineering Center under Grant No. DMR-1420645. The work at University of British Columbia was supported by the Natural Sciences and Engineering Research Council of Canada (NSERC) and Canada Research Chairs program. Parts of the research were performed at the Canadian Light Source, which is funded by the Canada Foundation for Innovation, NSERC, the National Research Council Canada, the Canadian Institutes of Health Research, the Government of Saskatchewan, Western Economic Diversification Canada, and the University of Saskatchewan. The research was also supported by the Global Frontier Program through the Global Frontier Hybrid Interface Materials (GFHIM) of the National Research Foundation of Korea funded by the Ministry of Science, ICT and Future Planning (2013M3A6B1078872).

- [1] N. Mott, *Metal-Insulator Transitions* (Taylor & Francis, London, 1974).
- [2] M. Imada, A. Fujimori, and Y. Tokura, *Rev. Mod. Phys.* **70**, 1039 (1998).
- [3] J. B. Torrance, P. Lacorre, A. I. Nazzari, E. J. Ansaldo, and C. Niedermayer, *Phys. Rev. B* **45**, 8209 (1992).
- [4] J. A. Alonso, J. L. Garcia-Munoz, M. T. Fernandez-Diaz, M. A. G. Aranda, M. J. Martinez-Lope, and M. T. Casais, *Phys. Rev. Lett.* **82**, 3871 (1999).
- [5] M. L. Medarde, *J. Phys. Condens. Matter* **9**, 1679 (1997).
- [6] R. J. Green, M. W. Haverkort, and G. A. Sawatzky, *Phys. Rev. B* **94**, 195127 (2016).
- [7] T. Mizokawa, D. I. Khomskii, and G. A. Sawatzky, *Phys. Rev. B* **61**, 11263 (2000).
- [8] H. Park, A. J. Millis, and C. A. Marianetti, *Phys. Rev. Lett.* **109**, 156402 (2012).
- [9] S. Johnston, A. Mukherjee, I. Elfimov, M. Berciu, and G. A. Sawatzky, *Phys. Rev. Lett.* **112**, 106404 (2014).
- [10] V. Bisogni, S. Catalano, R. J. Green, M. Gibert, R. Scherwitzl, Y. Huang, V. N. Strocov, P. Zubko, S. Balandeh, and J.-M. Triscone *et al.*, *Nat. Commun.* **7**, 13017 (2016).
- [11] G. Catalan, R. M. Bowman, and J. M. Gregg, *Phys. Rev. B* **62**, 7892 (2000).
- [12] R. Scherwitzl, P. Zubko, I. G. Lezama, S. Ono, A. F. Morpurgo, G. Catalan, and J. M. Triscone, *Adv. Mater.* **22**, 5517 (2010).
- [13] J. Liu, M. Kareev, B. Gray, J. W. Kim, P. Ryan, B. Dabrowski, J. W. Freeland, and J. Chakhalian, *Appl. Phys. Lett.* **96**, 233110 (2010).
- [14] D. Meyers, S. Middey, M. Kareev, M. van Veenendaal, E. J. Moon, B. A. Gray, J. Liu, J. W. Freeland, and J. Chakhalian, *Phys. Rev. B* **88**, 075116 (2013).
- [15] F. Conchon, A. Boulle, R. Guinebretiere, E. Dooryhee, J. L. Hodeau, C. Girardot, S. Pignard, J. Kreisel, F. Weiss, L. Libralesso, and T. L. Lee, *J. Appl. Phys.* **103**, 123501 (2008).
- [16] Y. Kumar, R. J. Choudhary, S. K. Sharma, M. Knobel, and R. Kumar, *Appl. Phys. Lett.* **101**, 132101 (2012).
- [17] J. Liu, M. Kargarian, M. Kareev, B. Gray, P. J. Ryan, A. Cruz, N. Tahir, Y.-D. Chuang, J. Guo, J. M. Rondinelli, J. W. Freeland, G. A. Fiete, and J. Chakhalian, *Nat. Commun.* **4**, 2714 (2013).
- [18] E. Mikheev, A. J. Hauser, B. Himmetoglu, N. E. Moreno, A. Janotti, C. G. Van de Walle, and S. Stemmer, *Sci. Adv.* **1**, e1500797 (2015).
- [19] J. Chakhalian, J. M. Rondinelli, J. Liu, B. A. Gray, M. Kareev, E. J. Moon, N. Prasai, J. L. Cohn, M. Varela, I. C. Tung, M. J. Bedzyk, S. G. Altendorf, F. Strigari, B. Dabrowski, L. H. Tjeng, P. J. Ryan, and J. W. Freeland, *Phys. Rev. Lett.* **107**, 116805 (2011).
- [20] U. Staub, G. I. Meijer, F. Fauth, R. Allenspach, J. G. Bednorz, J. Karpinski, S. M. Kazakov, L. Paolasini, and F. d'Acapito, *Phys. Rev. Lett.* **88**, 126402 (2002).
- [21] M. K. Stewart, J. Liu, M. Kareev, J. Chakhalian, and D. N. Basov, *Phys. Rev. Lett.* **107**, 176401 (2011).
- [22] J. Liu, M. Kareev, D. Meyers, B. Gray, P. Ryan, J. W. Freeland, and J. Chakhalian, *Phys. Rev. Lett.* **109**, 107402 (2012).
- [23] M. H. Upton, Y. Choi, H. Park, J. Liu, D. Meyers, J. Chakhalian, S. Middey, J.-W. Kim, and P. J. Ryan, *Phys. Rev. Lett.* **115**, 036401 (2015).
- [24] R. Scherwitzl, S. Gariglio, M. Gabay, P. Zubko, M. Gibert, and J. M. Triscone, *Phys. Rev. Lett.* **106**, 246403 (2011).
- [25] A. Tiwari and K. P. Rajeev, *Solid State Commun.* **109**, 119 (1999).
- [26] I. V. Nikulin, M. A. Novojilov, A. R. Kaul, S. N. Mudretsova, and S. V. Kondrashov, *Mater. Res. Bull.* **39**, 775 (2004).
- [27] U. Aschauer, R. Pfenninger, S. M. Selbach, T. Grande, and N. A. Spaldin, *Phys. Rev. B* **88**, 054111 (2013).
- [28] H. Y. Hwang, Y. Iwasa, M. Kawasaki, B. Keimer, N. Nagaosa, and Y. Tokura, *Nat. Mater.* **11**, 103 (2012).

- [29] R. J. Cava, B. Batlogg, C. H. Chen, E. A. Rietman, S. M. Zahurak, and D. Werder, *Nature (London)* **329**, 423 (1987).
- [30] J. P. Velez, K. D. Belashchenko, S. S. Jaswal, and E. Y. Tsymlal, *Appl. Phys. Lett.* **90**, 072502 (2007).
- [31] T. R. Paudel, S. S. Jaswal, and E. Y. Tsymlal, *Phys. Rev. B* **85**, 104409 (2012).
- [32] M. P. Warusawithana, C. Richter, J. A. Mundy, P. Roy, J. Ludwig, S. Paetel, T. Heeg, A. A. Pawlicki, L. F. Kourkoutis, M. Zheng, M. Lee, B. Mulcahy, W. Zander, Y. Zhu, J. Schubert, J. N. Eckstein, D. A. Muller, C. S. Hellberg, J. Mannhart, and D. G. Schlom, *Nat. Commun.* **4**, 2351 (2013).
- [33] H. Jeon, W. S. Choi, M. D. Biegalski, C. M. Folkman, I. C. Tung, D. D. Fong, J. W. Freeland, D. Shin, H. Ohta, M. F. Chisholm, and H. N. Lee, *Nat. Mater.* **12**, 1057 (2013).
- [34] A. J. Hauser, E. Mikheev, N. E. Moreno, J. Hwang, J. Y. Zhang, and S. Stemmer, *Appl. Phys. Lett.* **106**, 092104 (2015).
- [35] The disproportionation in the insulating phase of  $RNiO$  has been termed both *charge* and *bond* disproportionation [6–10]. The specific viewpoint is not critical for our results, so we simply refer to the phenomenon as disproportionation without labelling it as a specific type.
- [36] See Supplemental Material at <http://link.aps.org/supplemental/10.1103/PhysRevB.101.121105> for additional details, which includes Refs. [37–44,52,53].
- [37] S. Lany, *Phys. Rev. B* **78**, 245207 (2008).
- [38] V. Stevanović, S. Lany, X. Zhang, and A. Zunger, *Phys. Rev. B* **85**, 115104 (2012).
- [39] G. Kresse and D. Joubert, *Phys. Rev. B* **59**, 1758 (1999).
- [40] G. Kresse and J. Furthmüller, *Phys. Rev. B* **54**, 11169 (1996).
- [41] P. E. Blöchl, *Phys. Rev. B* **50**, 17953 (1994).
- [42] J. P. Perdew, K. Burke, and M. Ernzerhof, *Phys. Rev. Lett.* **77**, 3865 (1996).
- [43] V. I. Anisimov, F. Aryasetiawan, and A. I. Lichtenstein, *J. Phys. Condens. Matter* **9**, 767 (1997).
- [44] S. L. Dudarev, G. A. Botton, S. Y. Savrasov, C. J. Humphreys, and A. P. Sutton, *Phys. Rev. B* **57**, 1505 (1998).
- [45] S. J. May, J. W. Kim, J. M. Rondinelli, E. Karapetrova, N. A. Spaldin, A. Bhattacharya, and P. J. Ryan, *Phys. Rev. B* **82**, 014110 (2010).
- [46] E. Poindexter and A. A. Giardini, *Phys. Rev.* **110**, 1069 (1958).
- [47] D. Fuchs, E. Arac, C. Pinta, S. Schuppler, R. Schneider, and H. V. von Lohneysen, *Phys. Rev. B* **77**, 014434 (2008).
- [48] R. A. Rao, Q. Gan, C. B. Eom, R. J. Cava, Y. Suzuki, J. J. Krajewski, S. C. Gausepohl, and M. Lee, *Appl. Phys. Lett.* **70**, 3035 (1997).
- [49] Y. S. Kim, J. S. Choi, J. Kim, S. J. Moon, B. H. Park, J. Yu, J.-H. Kwon, M. Kim, J.-S. Chung, T. W. Noh, and J.-G. Yoon, *Appl. Phys. Lett.* **97**, 242907 (2010).
- [50] L. Wang, S. Dash, L. Chang, L. You, Y. Feng, X. He, K. Jin, Y. Zhou, H. G. Ong, P. Ren, S. Wang, L. Chen, and J. Wang, *ACS Appl. Mater. Interfaces* **8**, 9769 (2016).
- [51] T. J. Asel, H. Gao, T. J. Heisl, D. Adkins, P. M. Woodward, J. Hoffman, A. Bhattacharya, and L. J. Brillson, *J. Vac. Sci. Technol. B* **33**, 04E103 (2015).
- [52] K. Ogasawara, T. Miyamae, I. Tanaka, and H. Adachi, *Mater. Trans.* **43**, 1435 (2002).
- [53] R. J. O. Mossaneck, G. Domínguez-Cañizares, A. Gutiérrez, M. Abbate, D. Díaz-Fernández, and L. Soriano, *J. Phys: Condens. Matter* **25**, 495506 (2013).
- [54] C. Piamonteze, H. C. N. Tolentino, F. C. Vicentin, A. Y. Ramos, N. E. Massa, J. A. Alonso, M. J. Martínez-Lope, and M. T. Casais, *Surf. Rev. Lett.* **09**, 1121 (2002).
- [55] C. Piamonteze, F. M. F. de Groot, H. C. N. Tolentino, A. Y. Ramos, N. E. Massa, J. A. Alonso, and M. J. Martínez-Lope, *Phys. Rev. B* **71**, 020406(R) (2005).
- [56] J. W. Freeland, M. van Veenendaal, and J. Chakhalian, *J. Electron. Spectrosc. Relat. Phenom.* **208**, 56 (2015).